Title

Long term variations of summer rainfall over China and its possible link to global sea-surface temperature variability

Authors

Weng, H
Lau, W
Xue, Y

Publication Date

1999

Peer reviewed

Journal of the Meteorological Society of Japan, Vol. 77, No. 4, pp. 845–857, 1999

Multi-Scale Summer Rainfall Variability Over China and its Long-Term Link to Global Sea Surface Temperature Variability

By Hengyi Weng

Laboratory for Atmospheres, NASA/GSFC, Greenbelt, MD, U.S.A.
General Science Corporation/SAIC, Laurel, MD, U.S.A.

K.-M. Lau

Laboratory for Atmospheres, NASA/GSFC, Greenbelt, MD, U.S.A.

and

Yongkang Xue

Department of Geography, University of Maryland, College Park, MD, U.S.A.

(Manuscript received 21 July 1998, in revised form 17 May 1999)

Abstract

Multi-scale summer (Jun–Aug) rainfall variability over China and its long-term link to global sea surface temperature (SST) variability are studied for the period of 1955–1997. First, the dominant spatial and temporal patterns of the observed rainfall anomaly are studied by empirical orthogonal function (EOF) analysis. By a wavelet transform, interannual and decadal-interdecadal variabilities as well as a trend are found, with different dominance, in the first two EOF modes. EOF1 shows a sudden shift in rainfall anomaly over China in the late 1970s, representing overall wetter conditions in central China and drier conditions in northern and southern China in the 1980s than the conditions in the 1960s. This sudden shift is associated with a quasi-in-phase reinforcement between bidecadal and quadridecadal variabilities. EOF2 represents an increasing trend in the rainfall anomaly in broad central and southern China, especially in the Yangtze River valley, without an apparent shift in the late 1970s. The lack of such a shift is associated with an out-of-phase partial cancellation between a bidecadal cycle and the trend around that time.

Second, to understand the long-term rainfall variability that is linked to global SST variability, the singular value decomposition (SVD) analysis for the two fields is carried out. SVD1 links drought conditions in northern China and flood conditions in central China to an El Niño-like SST anomaly distribution. This mode shows both an apparent trend and a regime shift in the late 1970s, which do not coexist in the rainfall EOF modes. SVD2 links the rainfall anomaly in the area between the Yangtze River and the Yellow River and the opposite anomaly in southern China to a wave-like SST anomaly distribution in the eastern Pacific from tropics to extratropics. SVD3 links the rainfall anomaly in the Yangtze River valley to the SST anomaly in the western Pacific centered near 20°N 140°E. The rainfall variability in different areas of China that can be attributed to SST effects results from the interplay of the SVD modes. The most significant links found from SVD analysis are verified by cross-correlation functions. A scenario for a long-term link on the trend scale between the rainfall over China and global SST variabilities, through the associated large-scale circulation, is presented.

Corresponding author: Hengyi Weng, Laboratory for Atmospheres, NASA/GSFC, Greenbelt, MD, U.S.A. E-mail: weng@climate.gsfc.nasa.gov.

1. Introduction

The long-term variability of the Earth's ocean-atmosphere system has been the subject of many previous studies (Trenberth, 1990; Kawamura, 1994; Kleeman *et al.*, 1996; Zhang *et al.*, 1997; Lau and Weng, 1999, hereafter referred to as LW). In addition to a warming trend during the past four decades, one of the key features noted in these studies is a sudden regime shift in the late 1970s in the global climate state characterized by warming in the tropical oceans. This shift has been linked to decadal and interdecadal climate variability over North Pacific and parts of North America (Trenberth and Hurrell, 1994; Graham, 1994; Minobe, 1997). A similar variation has also been observed in regional summer rainfall over East Asia. There is also a trend during the past four decades with a regime shift in the late 1970s in the rainfall anomaly over some areas of China. A shift from a dry condition to a wet condition in central eastern China, and an opposite shift in northern China were found (Liang *et al.*, 1992; Chen *et al.*, 1994; Yatagai and Yasunari, 1995; Simmonds *et al.*, 1996; Nitta and Hu, 1996; Hu, 1997). Given the close timing between the global climate change and the East Asian monsoon variation, it is possible that the rainfall regime shift over the Asian monsoon region, in particular over China, may be linked to the global SST change. Despite these earlier findings, the relationship between the rainfall variability over China and the global SST variability has not been adequately explored, and is a focus of this work.

To explore this relationship, we first study the spatial and temporal variabilities of the summer rainfall anomaly over China. Then, we further study the part of the rainfall variabilities that are possibly linked to the global SST variability. Section 2 presents the data sets and the methods used. Section 3 shows the spatial and temporal rainfall patterns in China by empirical orthogonal function (EOF) analysis, and their temporal multi-scale nature by a wavelet transform. Section 4 presents the relationship between the rainfall and global SST anomalies based on singular value decomposition (SVD) analysis and cross-correlation functions. Section 5 provides a scenario for the long-term link between the variabilities of the rainfall over China and the global SST through the associated large-scale circulation. The final section briefly summarizes the results.

2. Data and methods

Analysis of the summer rainfall (the total amount for June, July and August) over China is based on a 160-station monthly data set for the period of 1955–1997 provided by Beijing University, China. Analysis of the summer SST for the same period is based on the monthly $10° \times 10°$ SST data provided by the National Oceanic and Atmospheric Administration (NOAA). The monthly $1° \times 1°$ COADS (Comprehensive Ocean-Atmosphere Data Set) surface horizontal wind data for the period of 1955–1993 are also used to establish a possible link between the long-term summer rainfall in China and the global SST variation. The domain for analyzing SST is limited within the latitudes of 40°S–60°N, while that for the surface wind is 40°S–40°N.

For the rainfall and SST anomaly fields, the climatological seasonal cycles, defined by the averaged annual cycle for the data period, have been removed before EOF and SVD analyses are applied. In the temporal domain, each principal component (PC) from EOF and SVD analyses is scaled by its standard deviation (σ). The corresponding spatial pattern is then multiplied by its PC's standard deviation. Thus, the EOF or SVD spatial coefficients represent approximately the 1-σ loading of that component. A Morlet wavelet analysis is used to identify various timescales, defined as one full period, in the PCs of the first two EOF modes. The standard procedures of these methods will not be presented. The interested readers are referred to North (1984) for EOF, to Brentherton *et al.* (1992) and Wallace *et al.* (1992) for SVD, and Weng and Lau (1994) and Lau and Weng (1995) for the Morlet wavelet transform used here.

3. Spatial and temporal rainfall patterns

3.1 Dominant EOF patterns

The spatial patterns and their corresponding PCs of the first two EOF modes are shown in Fig. 1. EOF1 explains 15.1 % of the total summer rainfall variance in China. Its spatial pattern shows that the variation of the summer rainfall in central-eastern China (29°–35°N, 105°–120°E), including the Yangtze River valley (YRV, 29°–32°N, 105°–120°E) and Huaihe River valley, is opposite to the variabilities in the areas to its south and north. The rainfall anomaly in the northern part of northeastern China varies with a similar tendency as that in central-eastern China. A prominent character of PC1 is the sudden regime shift in the late 1970s, from overall negative anomalies between the late 1950s and the late 1970s to overall positive anomalies between the late 1970s and the beginning of the 1990s. However, there is no apparent trend for the data period in PC1.

EOF2 explains 11.0 % of the total summer rainfall variance in China. Its spatial pattern shows that when the broad central and southern China, especially the YRV, is wetter, the area to the north is slightly drier. There seems to be a trend for the data period, emphasized by persistent, large, negative anomalies in the earlier period (between the mid-1950s and the late 1960s), and persistent, large,

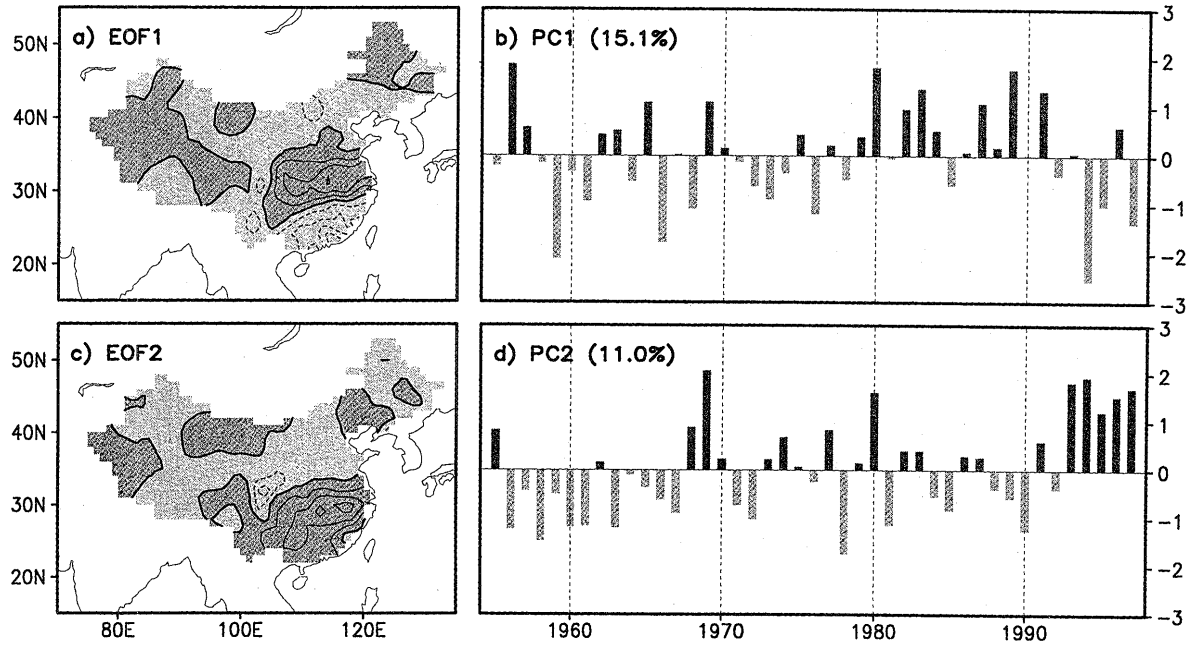

Fig. 1. Spatial patterns of EOF1 (15.1 %) and EOF2 (11.0 %) and their corresponding PCs of China summer rainfall anomaly. The contour interval in spatial patterns is 40 mm. The positive (negative) values are dark (light) shaded. The results have been scaled by each PC's standard deviation.

positive anomalies in the later period (since the beginning of the 1990s). There is no apparent regime shift in the late 1970s in PC2.

The difference between the temporal characteristics of the two PCs is apparent. PC1 exhibits a rather sudden regime shift in the late 1970s without much of the trend signal for the data record, while PC2 exhibits a trend without an apparent shift in the late 1970s. In the areas where the spatial coefficients in the two EOF patterns are both positive (*e.g.*, the YRV), the combination of the two EOF modes may imply an increasing rainfall trend (due to EOF2), with a sudden regime shift in the late 1970s (due to EOF1). In the areas with both negative spatial coefficients (*e.g.*, northern China), a decreasing trend in rainfall with an opposite shift may be found.

Different temporal behaviors of PC1 and PC2 may be manifestation of different phase and intensity combinations of multi-scale temporal rainfall variabilities. The two PCs seem to vary on interannual and decadal-interdecadal timescales as well as a trend scale with different dominance. These timescales will be analyzed in detail by the Morlet wavelet transform in the following subsection.

The EOF patterns presented here are somewhat different from those presented by Nitta and Hu (1996), who used a rainfall data set from the same 160 stations. The difference is mainly due to different data periods and methods used. The data set used by Nitta and Hu (1996) covered the severe flood in YRV in 1954, but not the severe flood in southern China during the intense 1997 El Niño event. The data set used here includes 1997, but not 1954. The inclusion or exclusion of a severe flood year in a data set that is not very long will have some impact on the dominant EOF patterns. Furthermore, the rainfall data they analyzed are normalized. It actually amplifies the contribution of the rainfall variability in arid and semi-arid areas to the overall patterns of the leading EOF modes. The rainfall data analyzed here are not normalized. The results presented here emphasize the rainfall variabilities in the areas where rainfall is abundant, and severe flood effects are most devastating.

3.2 Multiple timescales in rainfall variability

Figure 2 shows the real part of the Morlet wavelet coefficients of the first two PCs for the timescales between 2 and 128 years during the 43 years.[1] The signals with large variability are mainly on the shorter, interannual timescales. Since longer-term variabilities may be seen as a background of shorter-term ones, we proceed with the discussion of the rainfall variabilities from longer to shorter timescales.

In PC1 (Fig. 2a), the trend signal on the longest timescale is very weak. A quadridecadal cycle (around 45 years here) is found, which changes

1 Since wavelet transform is capable to find local signals, a signal with a timescale longer than the data record could also be found as a projection of the time series onto a wavelet base function with such a timescale. An ascending or descending part of an oscillating variability cycle with its half-cycle longer than the data record may be considered as a trend signal for the data record.

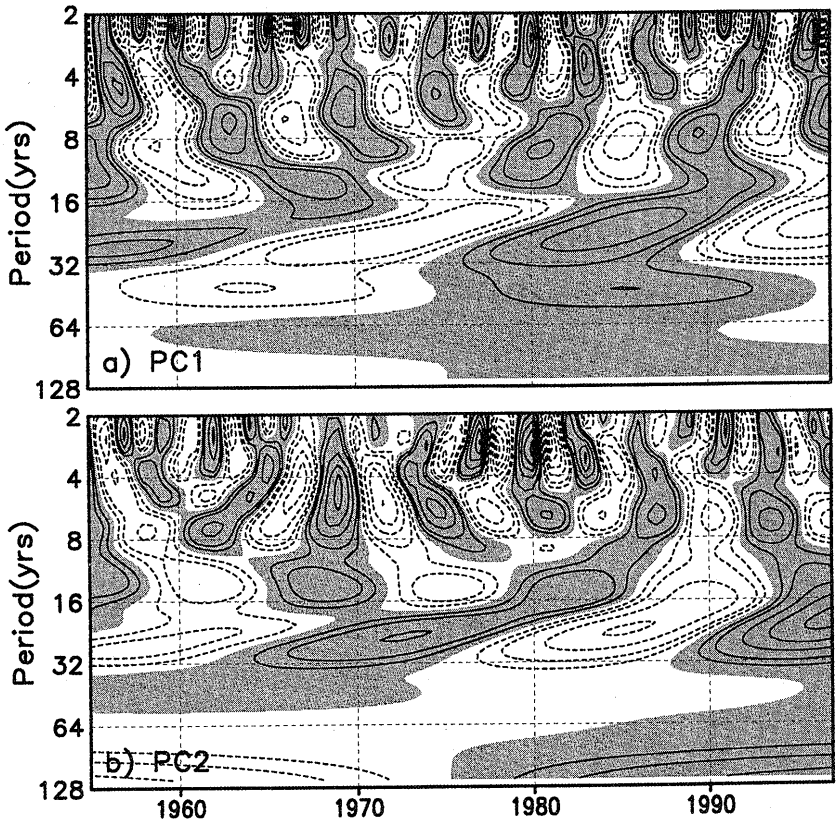

Fig. 2. Wavelet coefficients are for (a) PC1 and (b) PC2 of the EOF modes. Shaded areas are for positive values. Contour interval is 0.2 with the extra contour line at 0.1 for both signs. 0-line is omitted for clarity.

phase from negative to positive around the mid-1970s. Also found is a pronounced bidecadal signal, which seems to have three main components with timescales of 27, 22 and 19 years. The 27yr component is stronger among the three in the 1950s. It gradually gives way to the components with shorter timescales, until the 19yr component becomes dominant in the 1990s. The bidecadal signal switches phase in the mid-1960s, the late 1970s, and the beginning of the 1990s. The time when the stronger bidecadal signal changes phase in the late 1970s is close to the time when the weaker quadridecadal signal changes phase in the mid-1970s. The quasi-in-phase reinforcement of these two timescales, with the much less contribution from the very weak trend, is associated with the sudden regime shift in overall rainfall anomalies in the late 1970s for PC1 (see Fig. 1b).

The situation in PC2 (Fig. 2b) is quite different. There is a clear trend signal in PC2. The trend changes phase from negative to positive in the mid-1970s. There is no obvious quadridecadal signal in PC2. However, the bidecadal signal in PC2 is stronger than, and out-of phase to, its counterpart in PC1. Similar to PC1, the timescale of the bidecadal signal decreases from about 27 years in the 1950s to 22 years in the 1970s and 1980s, and continues decreasing in the 1990s. The decrease in timescale of the bidecadal signal may also be understood by the tendencies that the 27yr component is weakening while the 19yr component is strengthening from the 1950s to the 1990s. The bidecadal signal changes phase in the mid-1960s, the late 1970s and the beginning of the 1990s, and is out of phase with the trend in the late 1970s. The partial cancellation between the two scales in PC2 blurs the shift in the late 1970s, which is so apparent in PC1. However, the bidecadal signal is in phase with the trend signal in the period between the mid-1950s and the mid-1960s, and the period since the beginning of the 1990s. The quasi-in-phase reinforcement between the two timescales during these two periods results in persistent, large, negative anomalies in southern China, especially in the YRV in the earlier period while persistent, large, positive anomalies in the later period.

Thus, the bidecadal signals in both PCs are important components affecting the regime shift in the late 1970s in PC1 and the trend in PC2. It is expected that the combination of the two leading EOF modes would represent different dominance of longer timescales in rainfall anomaly in different regions of

China. In the areas where both spatial coefficients in the two EOF modes are either positive or negative simultaneously, the bidecadal signal is weakened due to partial cancellation between the two modes. But, the trend signal and the shift in the late 1970s may coexist due to the quasi-in-phase of the quadridecadal signal in PC1 and the trend signal in PC2. In the areas where the spatial coefficients in the two EOF modes are opposite, the bidecadal signal and, therefore, the shifts in the mid-1960s and the beginning of the 1990s are enhanced. The trend signal may be weakened due to partial cancellation between the quadridecadal signal in PC1 and the trend signal in PC2. The shift in the late 1970s for a given area may be either enhanced or weakened depending on the relative magnitudes of the spatial and temporal coefficients in the two modes. The timing of the shift may actually vary in a few years from the mid-1970s to the late 1970s, depending on the relative intensity of these longer timescales in different locations. For simplicity, we specify such a shift in the "late" 1970s in our discussion.

It is expected that some features of the rainfall variability on shorter timescales (decadal and interannual timescales) may also be different before and after regime shift in the late 1970s. For convenience, we denote the time periods of 1955–1977 and 1978–1997 as Period I and Period II, respectively, in the following discussions.

The decadal signal in PC1 is quite nonstationary. Its timescale varies basically between 10 and 14 years. The 14yr component is mainly seen in Period I, when the 27yr component is relatively strong. The 10yr component undergoes a frequency modulation by longer timescales, crossing the boundary between the decadal and interannual timescale bands in the early 1960s and the late 1980s. Because of its relatively short cycle length, the decadal variability in PC1 may not play an important role in the regime shift from Period I to Period II. Its quasi-in-phase relationship with the bidecadal and quadridecadal variability does enhance the suddenness of such a regime shift in the late 1970s.

In PC2, the 14yr component is relatively stationary during Period I. The two PCs are basically in-phase on the 14yr timescale during Period I. There is little signal in the 10yr component in PC2.

The dominant interannual timescales in the two PCs are found near the subharmonics of the annual cycle. The wavelet coefficients of PC1 are mainly clustered in two timescale bands: the longer one is between 4 and 8 years, and the shorter one between 2 and 4 years. Both vary in intensity and length with time. As mentioned earlier, the longer interannual variability shows some interplay with decadal variability. When the 10yr component reduces its length to a component having a timescale shorter than 8 years, a 4.8yr component reduces its length to 4 years or less. The variability in the shorter interannual band is the strongest among all timescales. The dominant timescale is between 2.2–2.6 years in Period I, representing a quasi-biennial oscillation (QBO) signal. In Period II, beside the QBO signal, there is a secondary dominant timescale between 3 and 4 years, which is quite nonstationary.

The behavior of the interannual variability of PC2 is also different from that of PC1. In the longer interannual band, there are two dominant timescales, around 5 and 7 years at the beginning of Period I. These components gradually change their lengths and finally merge to a single component with a timescale of 5.6-yr at the end of Period I. This 5.6yr component then increases its length to 6.7 years, and becomes quite stationary throughout Period II. In the short interannual band, QBO is overall dominant in the whole data period, but not as intensive as that in PC1. A 3.3yr component is only dominant in the early Period II.

The averaged interannual timescale in both PCs is about 4 years, with the dominance of QBO. This timescale is similar with the averaged El Niño timescale of 4 years documented by Trenberth (1997). The individual positive peaks in PC1 or PC2 (Figs. 1b and 1d) do not correspond well one-to-one with El Niño events observed in the SST anomaly in the eastern tropical Pacific. Thus, the first two EOF modes may not separately link the summer rainfall variability over China to SST variability on interannual and longer timescales. The links between the rainfall and SST variabilities, on all timescales, may be found by a method that is able to detect dominant spatial and temporal patterns from the coupled variabilities between the two fields. SVD analysis is a proper tool for such a purpose, and is applied in the next section.

4. Correlation analyses

The relationship between the (spatial and temporal) variabilities of the summer rainfall over China and the global SST is first carried out by SVD analysis. Then, the cross-correlation functions between several area-averaged rainfall and SST anomaly time series are calculated and compared to verify some of the links found by SVD.

4.1 Coupled rainfall-SST modes

The first three SVD modes will be examined here (Fig. 3). In the following discussion, we use the suffix r and s to denote the rainfall and SST anomaly fields, respectively. The description for a spatial pattern is for the time when the corresponding PC is positive, if not specified otherwise.

SVD1 explains 35.1 % of the total squared covariance between the rainfall and SST anomaly fields. The SVD1s spatial pattern (Fig. 3a1) shows an El Niño-like structure with positive anomalies in the

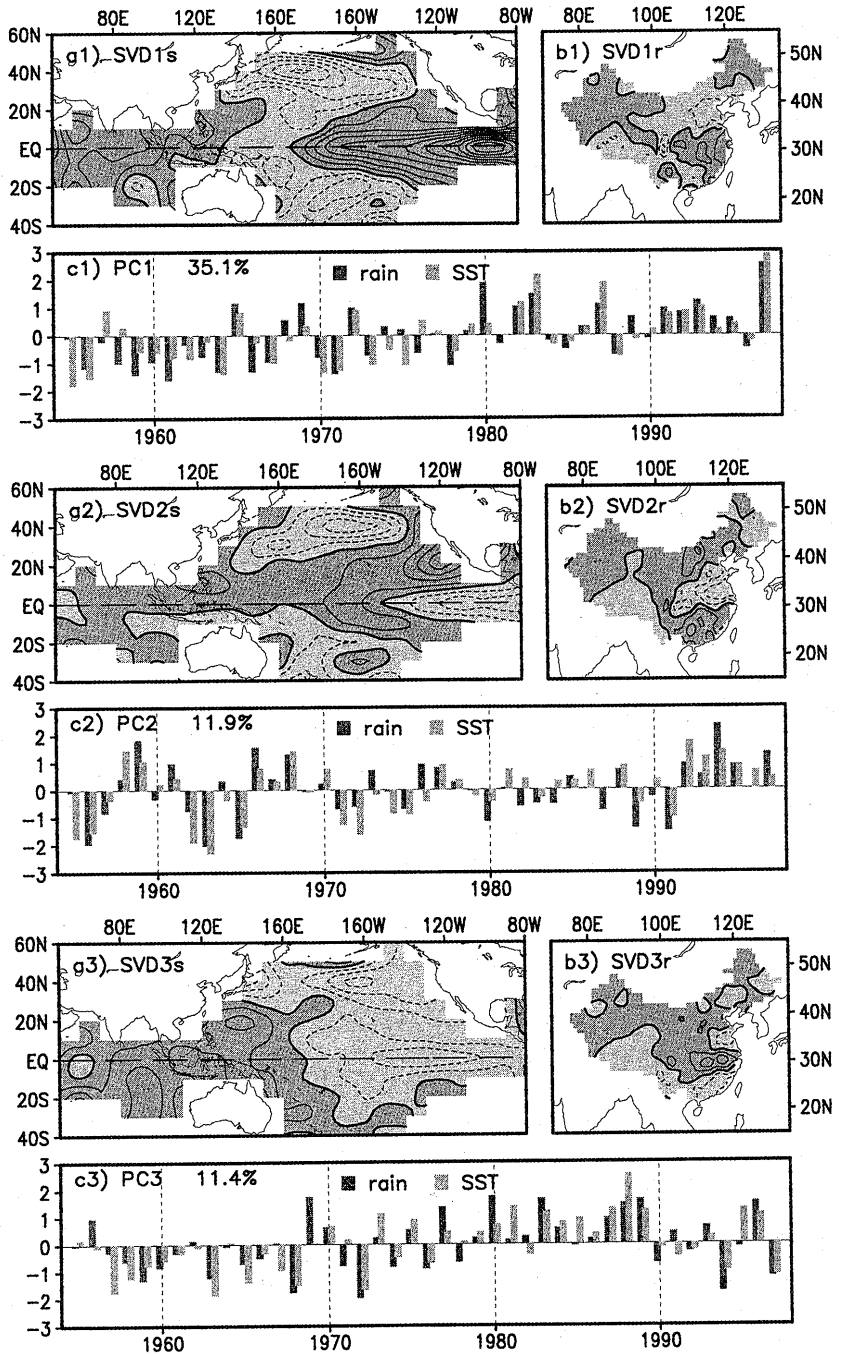

Fig. 3. The SVD modes for (a) SST spatial pattern, (b) summer China rainfall spatial pattern and (c) the corresponding PCs. SVD1 (35.1 %) (upper panels), SVD2 (11.9 %) (middle panels), and SVD3 (11.4 %) (lower panels). The contour interval in (a) is 0.1°C, and that in (b) is 40 mm. The results have been scaled by the standard deviation of each PC.

eastern tropical Pacific and the Indian Ocean, and an extensive pool of abnormally cold water in the extratropical northern Pacific. Coupled with this SST pattern, a main feature of SVD1r (Fig. 3b1) is that central-eastern China, extending to the southeastern coastal area, and the upper northeastern China are wetter, while northern China, and a small portion of southern China are drier, than respective normal conditions. The SVD1s spatial pattern is similar to that of the EOF1 mode of the annual SST anomaly shown by LW, which represents an interannual mode modified by interdecadal variations and a global warming trend. The SVD1r spatial pattern seems to capture the main features of the first two rainfall EOF modes, as expected in the previous section.

There is an apparent trend with a regime shift of overall anomalies in the late 1970s in both PC1*s* and PC1*r* (Fig. 3c1). The extreme positive anomalies of both PC1*s* and PC1*r* in Period II apparently correspond to El Niño events. The magnitudes of the positive anomalies are reduced in Period I, because the El Niño signals during that time period are shadowed by the negative contributions from the trend and other long-term signals. The YRV and northern China seem to be key areas where the rainfall variabilities are related to the global climate change through SST variation. These two areas exhibit opposite rainfall trends for the data period.

SVD2 explains 11.9 % of the total squared covariance between the rainfall and SST anomaly fields. The SVD2*s* spatial pattern (Fig. 3a2) shows a wave train structure in the eastern North Pacific. The wave train consists of relatively colder water in the tropics and extratropics, and warmer water in subtropics off the southwest coast of North America. The SVD2*s* spatial pattern is similar to the EOF3 spatial pattern of the annual SST anomaly in LW. This wave train may indicate oceanic heat exchange by ocean circulation in the eastern part of North Pacific between tropics and extratropics. The SVD2*r* spatial pattern (Fig. 3b2) shows that when the water in the eastern tropical and extratropical Pacific is colder, and the water in between is warmer, the area between the Yangtze River and the Yellow River may be drier, while the Inner Mongolia and southern China are wetter. There is no apparent shift in the late 1970s, nor apparent positive anomalies corresponding to El Niño events in both PC2*s* and PC2*r* (Fig. 3c2). There are persistent positive anomalies in the 1990s, which is similar to the persistency of EOF2 during that time.

SVD3 explains 11.4 % of the total squared covariance between the rainfall and SST anomaly fields. The SVD3*s* spatial pattern (Fig. 3a3) is similar to the EOF2 spatial pattern of the annual SST anomaly in LW. This pattern may represent the cold tongue activity connected with the subduction of cold water from the extratropical Pacific (Gu and Philander, 1997). Associated with the eastern Pacific cold region is a SST dipole in the western Pacific, having a warm center in the south and a cold center in the north. This is similar to the Pacific-Japan pattern found by Nitta (1987) for intraseasonal variability. The warm center is around 20°N 140°E where the year-round SST anomaly in the Kuroshio Current has a positive correlation with "Mei-yu" rainfall in the middle and lower reaches of the Yangtze River (Lau and Li, 1984). The SVD3*r* spatial pattern (Fig. 3b3) shows a maximum positive rainfall anomaly along the Yangtze River, while a negative anomaly exists in the lower reaches of the Huaihe River and the southeastern and southern China. These spatial patterns of SVD3 are consistent with Lau and Li (1984). Both PC3*s* and PC3*r* (Fig. 3c3) show overall negative anomalies in the period between the late 1950s and the late 1960s, and overall positive anomalies in the 1980s, with no apparent persistency in the 1970s and 1990s.

SVD4 explains only 6.4 % of the total squared covariance and is well separated from SVD3. Since the first three modes explain almost 60 % of the total squared covariance, and shown the main features of the relationship between the rainfall and SST anomaly fields, higher modes will not be discussed here.

The rainfall over China that is linked to the global SST warming on the trend scale is reinforced by the three modes in the areas where the spatial coefficients have the same sign. The rainfall in northern China between the Huaihe River and the Yellow River, including Shandong Peninsula (36–37°N, 118–123°E), shows a decreasing trend during the past four decades. Meanwhile, the areas to the south of the Yangtze River and the upper northeastern China show increasing trends. Such trends with apparent regime shifts in the late 1970s are consistent with the combination of the first two EOF modes in the areas where spatial coefficients in the two EOF modes are either both positive (*e.g.*, the YRV) or both negative (*e.g.*, northern China). For the areas where the spatial coefficients have different signs among the three SVD modes, the net response of the rainfall to SST variability on the trend scale depends on the relative magnitudes of the temporal and spatial coefficients in Fig. 3. Thus, the resultant relationship between the regional rainfall anomaly over China and the global SST warming trend contains a large degree of reinforcement or cancellation among the first three SVD modes.

Similar interplay between the three SVD modes may also be seen on shorter timescales. For example, during El Niño summers, PC1*s* is always positive and PC1*r* is mostly positive, while the principal components in the second and third modes may not. Thus, the summer rainfall distribution in China during El Niño summers will be different from year to year, depending on the combinations of these rainfall SVD modes, or on different links to the SST anomaly field. This analysis may provide an explanation for the somewhat weak and varied El Niño signals in observed rainfall anomaly in many areas of China. The link between the summer rainfall anomaly over China and the global SST anomaly on interannual timescale, especially for the link between the 1997 El Niño event and the summer drought and flood in China, will be specially discussed in a separate paper.

The above discussed links between the variabilities of the rainfall over China and the global SST, presented by the SVD modes, are different from those obtained by Nitta and Hu (1996) and Hu

Table 1. Cross-correlation coefficients between area SST anomaly and China summer rainfall anomaly for the period of 1955–1997. The geographical specification of these areas is given in the text. The 90 %, 95 % and 99 % confidence levels are 0.25, 0.30 and 0.39, respectively. The coefficients above the 99 % level are in bold face.

Rain	SSTA			
	E. Pacific	*W. Pacific*	*N. Pacific*	*Indian Ocean*
YRV	0.21	**0.42**	−0.13	0.27
S. China	−0.10	0.10	0.01	0.04
N. China	**−0.59**	0.00	0.29	−0.18

(1997). Nitta and Hu (1996) and Hu (1997) performed SVD analysis between China's rainfall and temperature first, then calculated the correlation between the principal component of a rainfall SVD mode and the SST anomaly field. Thus, what they showed was a somewhat tangled relationship among all the three variables (rainfall and temperature over China and SST). That is different from the rainfall-SST relationship discussed here.

We will complement the SVD analysis by cross correlation functions between the rainfall anomalies in different areas of China and the SST anomalies in different oceanic areas in the following subsection.

4.2 Area-averaged correlation

The major loading centers shown in the rainfall and SST spatial patterns of the SVD modes are chosen for cross-correlation study. For the rainfall, three areas are chosen, *i.e.*, the YRV, southern China (22–25°N, 105–115°E), and northern China (36–41°N, 105–120°E). For SST, four oceanic areas are chosen, *i.e.*, the eastern tropical Pacific (Equator, 80°–110°W), the western subtropical Pacific (20°N, 130–150°E), the extratropical northern Pacific (40°N, 160°E–160°W), and the northern Indian Ocean (0–10°N, 80–100°E).

Table 1 shows the cross-correlation coefficients (ccf) between the area-averaged observed rainfall and SST anomalies. There are two coefficients above the 99 % significance level. A significant negative correlation ($ccf = -0.59$) is found between the rainfall anomaly in northern China and the SST anomaly in the eastern tropical Pacific. This highly negative correlation may be understood from the previously discussed interplay of the three leading SVD modes. The positive coefficient between the rainfall anomaly in northern China and the SST anomaly in the extratropical North Pacific ($ccf = 0.29$) almost reaches the 95 % confidence level. Apparently, the first SVD mode makes the most contribution to this correlation among the three modes.

A significant positive correlation ($ccf = 0.42$) is found between the rainfall anomaly in the YRV and the SST anomaly in the western subtropical Pacific, which is mainly linked by SVD3 and secondly by SVD1. It may reflect a stronger direct influence by the neighboring western subtropical Pacific on the rainfall anomaly in the YRV (Wu and Liu, 1995; Wu *et al.*, 1995). The rainfall anomaly in the YRV and the SST anomaly in the eastern tropical Pacific have a less significant positive correlation ($ccf = 0.21$). This is because the influences of the SST variabilities in the eastern tropical Pacific, represented by SVD1 and SVD3, on the rainfall anomaly in the YRV are opposite. It also shows the complexity in the timing of the occurrences of the floods in the YRV and El Niño events. The positive coefficient between the rainfall anomaly in the YRV and the SST anomaly in the Indian Ocean ($ccf = 0.27$) is above the 90 % confidence level. It is mainly due to the in-phase influence of the Indian Ocean SST on the rainfall in the YRV represented by SVD1 and SVD3.

The rainfall in southern China does not seem to have a close relationship with the SST variability in any of the oceanic areas shown in Table 1. It is possible that the summer rainfall in southern China may be influenced by local monsoon variability that is not closely related to the global SST variability, and/or there is a large cancellation in the influences by dominant large-scale SST anomalies in these regions; as revealed in previous subsections.

Note that the choice of the area for the eastern tropical Pacific studied in this section is based on the SST loading center in the eastern tropical Pacific in SVD1*s*, where mainly covers the eastern part of the Niño3 area. This is not exactly the same area used for the conventionally, or newly defined El Niño index (Trenberth, 1997). For comparison, Table 2 shows the cross-correlation coefficients between the SST anomalies in the Niño4, Niño3.4, Niño3, and Niño1–2 areas and the rainfall in the same areas in China as those shown in Table 1. The negative coefficients between the SST anomalies in these areas and rainfall in northern China are −0.27, −0.47, −0.57, and −0.54, respectively. These magnitudes are all less than their counterpart in Table 1. The summer rainfall anomaly in northern China seems to have a better simultaneous negative correlation to the SST anomaly in the far-eastern tropical Pacific, than the SST anomalies in the areas for the four El Niño indices during the past four decades.

Table 2. Cross-correlation coefficients between area SST anomaly in Niño4, Niño3.4, Niño3, as well as Niño1–2 and China summer rainfall anomaly in the same period and areas of China as in Table 1. The 90 %, 95 % and 99 % confidence levels are 0.25, 0.30 and 0.39, respectively. The coefficients above the 99 % level are in bold face.

Rain	SSTA			
	Niño4	*Niño3.4*	*Niño3*	*Niño1–2*
YRV	0.09	0.09	0.17	0.19
S. China	0.17	0.11	0.00	−0.11
N. China	−0.27	**−0.47**	**−0.57**	**−0.54**

5. Long-term link

To study the long-term rainfall-SST link on the trend timescale with a regime shift in the late 1970s, we take the half difference of the time-averaged SST anomaly (Fig. 4a), the rainfall anomaly (Fig. 4b), and the surface wind anomaly (Fig. 4c) between Period II and Period I, respectively.[2] These patterns basically represent the averaged anomaly situations in Period II. In Fig. 4a, the warmest area is found in the eastern tropical Pacific. The warm tongue extends toward the west, merging with a basin-wide positive anomaly in the tropical Pacific and the Indian Ocean. It is similar to the ENSO-like interdecadal pattern found by Zhang *et al.* (1997), especially to the trend pattern of annual SST anomaly in LW. The SST anomaly pattern in the eastern tropical Pacific during the warm phase of the trend shows a less-warm region in the Niño3 area, slightly to the west of the "cold core" in the eastern tropical Pacific found in SVD3*s* (Fig. 3a3).

The warm SST anomaly center in the western subtropical Pacific could be an important factor in determining the intensity and the location of the subtropical high in the northwestern Pacific. The latter may play an important role in the change in summer rainfall regime over China (Lau and Li, 1984; and Li and Liao, 1998). The rainfall pattern (Fig. 4b) shows a zonally oriented distribution, consisting of a major wet area along the Yangtze River and the drier areas to both of its northern and southern sides, as well as a slightly wetter area in the upper northeastern China. In the surface wind pattern (Fig. 4c), there is a convergence region near the warm center of the central equatorial Pacific around 160°W. To its west, there is anticyclonic wind originating from the southern Pacific off the eastern coast of Australia. The anticyclonic southeast wind turns to southwest wind after passing the divergent area over Indonesia near the Equator due to the earth's rotation effect. To the north of this divergent area, there is a cyclonic northeast wind toward East Asia. The thick dashed line in Fig. 4c indicates a "shear zone" where these anomaly winds might meet.

The combination of Figs. 4a–4c may suggest a possible long-term link between the anomalies of the summer rainfall over China, SST, and the large-scale wind circulation, encapsulated by the following scenario. In Period II, the increase in convergence in the central tropical Pacific over the area with positive SST anomaly (Figs. 4a and 4c) leads to an increase in ascending air over the region. By mass continuity, it results in a main descending motion over Indonesia, and a secondary descending motion over the Niño3 area, where there are less warm areas compared with their neighboring areas in the Tropics. The increased descending air enforces low-level divergence over these areas. The stronger divergence over Indonesia is associated with an anticyclonic southwest surface wind anomaly over the western Pacific, and the South China Sea. Over the western subtropical Pacific, the cyclonic center around 20°N 140°E is near the warm SST anomaly center in SVD1*s* (see Fig. 3a1). The cyclonic northeast wind anomaly over the East China Sea meets the moist southwest wind anomaly from the South China Sea, forming the shear zone near 30°N in the lower and middle reaches of the Yangtze River, as shown in Fig. 4c.

The convergence of the moist airflow in central China results in rainfall over the shear zone in the YRV. This mainly zonally oriented convergence forces secondary meridional circulation in eastern China. The airflow off the shear zone descends in the northern and southern regions to this convergence band, tending to dry the areas on both sides. The descending air in northern China will further induce ascending air over northeastern China, where rainfall is possible when moist air is supplied. Thus, the dynamic flow motion over China tends to result in a rainfall pattern with alternation of wet and dry bands from southern to northeastern China.

Meanwhile, there is an increase in the southwest summer monsoon over the Bay of Bengal. Such an increase in wind should correspond to an increased land-ocean temperature contrast between the land in southwestern China and the Indo-China Peninsula and the adjacent Indian Ocean. In Period II, the averaged temperature over the adjacent Indian Ocean is about 0.1°C higher, while the temperature over the land area is even higher, about 0.2°C, than their respective means over the 43 years (not shown).[3] Thus, the increased southwest summer monsoon is maintained by the increased land-ocean

2 The half-difference between the two periods is comparable with corresponding 1-σ anomaly in magnitude. Period II is truncated to 1993 due to lack of updated COADS wind data.

3 The result is based on the global 5° × 5° grid surface temperature data, provided by Dr. P. Jones at the web site http://www.cru.uea.ac.uk .

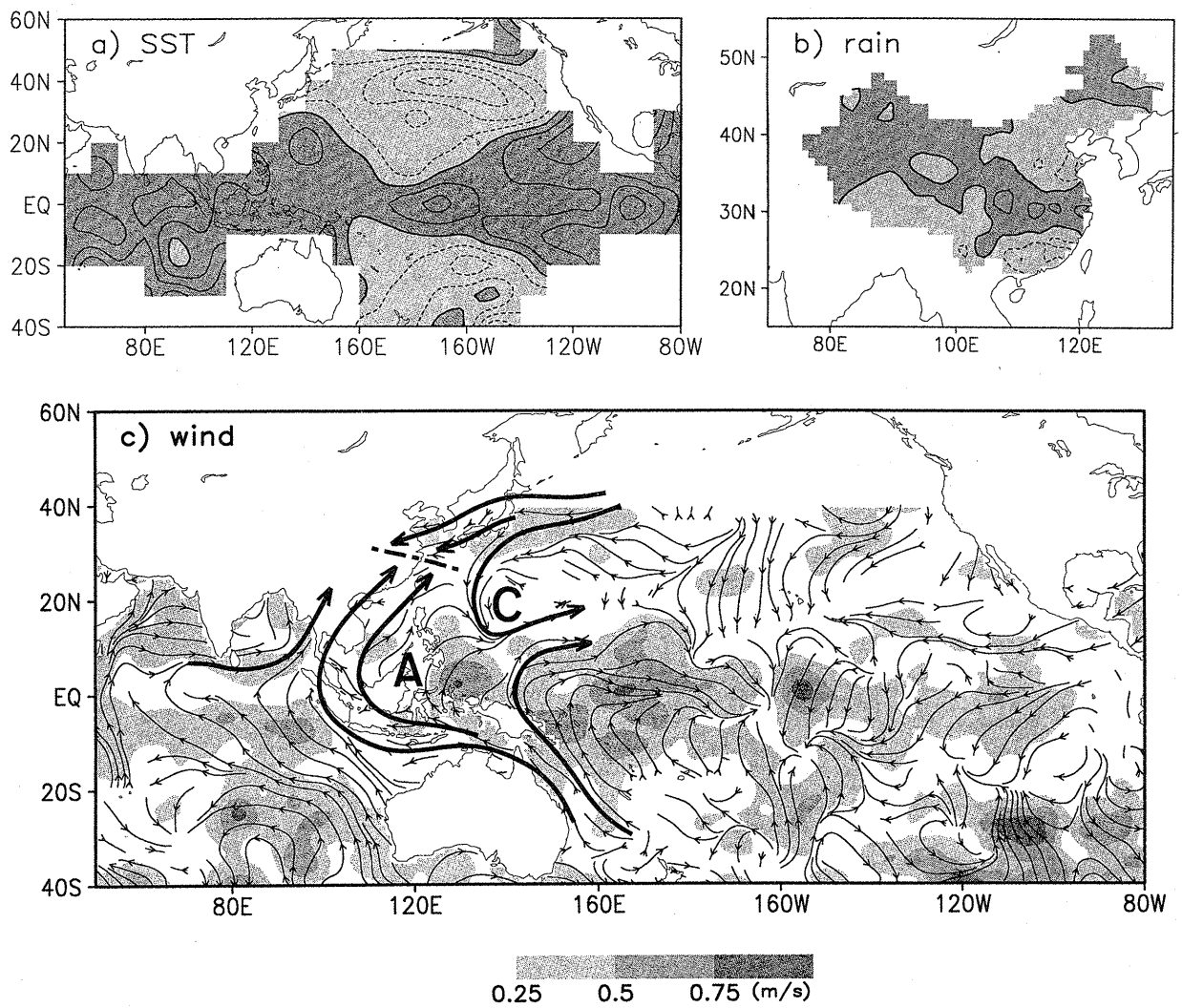

Fig. 4. The half-differences between Period II and Period I for (a) SST anomaly (contour interval: 0.1°C), (b) China rainfall anomaly (contour interval: 40 mm), and (c) the surface wind anomaly (unit: m/s). The patterns reflect the prevailing conditions during Period II. The thick lines with arrow indicate the *prevailing* surface airflow anomaly that may influence rainfall anomaly over China (small-scale local circulation is ignored here). The thick dashed line indicates where the airflow meets, which is near the shear zone discussed in the text.

temperature contrast during Period II. Moreover, the increase in the SST in the adjacent Indian Ocean itself may provide increased moisture contained in the airflow over there. Thus, during Period II, the southwest wind over the Bay of Bengal, which enters the southwestern China and the upper and middle reaches of the Yangtze River via Burma, is not only intensified but also brings more abundant moisture into central China. As seen in Fig. 4a, the SST anomaly in the Indian Ocean is in phase with the SST anomaly in the eastern tropical Pacific on the trend timescale. Thus, the southwest summer monsoon is intensified when the eastern tropical Pacific is warmer on the trend timescale. This relationship is different from that on the interannual timescale. In the latter case, the southwest summer monsoon is weak during El Niño years (Webster and Yang, 1992).

As shown in Table 1, there is no significant correlation between the rainfall anomaly in southern China and the SST anomaly in the oceanic areas chosen here. However, on the trend scale, while southern China is affected by increased anticyclonic moist flow over the South China Sea, the moist air may not lead to precipitation due to lack of convergence over there in Period II. Moreover, this area is under the influence of the meridionally descending air forced by the low-level convergence in YRV. The net effect of these factors may result in drier southern China in Period II, as shown in Fig. 4b.

During Period I, the above-discussed conditions are reversed. Note that all the terminology used for the description are in their relative sense with respect to the mean conditions averaged over the data

period. The oceanic locations discussed here are approximate because of the coarse resolution. However, this coarse-resolution SST data set does reveal the main features which are similar to those from other SST data sets with finer resolution (figures are not shown). The subtropical and extratropical North Pacific is the upstream of North America. It is reasonable to expect that the regime shift in the late 1970s in the rainfall anomaly may also link to the climate regime shift in North Pacific and North America (mentioned in Introduction) through SST variability. Thus, the regime shift in the late 1970s in the summer rainfall in China may be a manifestation of the global climate change.

6. Summary

The spatial and temporal summer rainfall variabilities over China for the period of 1955–97 are analyzed by EOF and wavelet analyses. The links between the variabilities of the rainfall and the global SST are studied by SVD, complemented by cross-correlation functions. The key findings are as follows.

1) Each of the first two EOF modes of the summer rainfall variability over China exhibits selective multiple timescales. The apparent regime shift in the late 1970s in PC1 is associated with the quasi-in-phase reinforcement between the bidecadal and quadridecadal signals. The decadal signal in PC1 enhances the suddenness of the shift. The persistent negative anomalies in the 1960s, and the persistent positive anomalies in the 1990s in PC2, are associated with the reinforcement between the bidecadal and trend signals. There is no apparent shift in the late 1970s in PC2, associated with the partial cancellation between the two signals.

2) SVD1 shows the apparent trends and the sudden regime shifts in the late 1970s in both rainfall and SST fields, which do not coexist in the rainfall EOF modes. The response of the regional rainfall over China to the global SST variability contains a large degree of reinforcement or cancellation among the first three SVD modes. Northern China and the YRV are found as two key regions having close links to SST variability. The rainfall anomaly in northern China is negatively correlated to the SST anomaly in the eastern tropical Pacific, while that in the YRV is positively correlated to the SST anomaly in the western subtropical Pacific.

3) On the trend scale, the abundant rainfall in the YRV is not only due to the moist air from the western Pacific, but also to increased moist southwest monsoon. When the eastern tropical Pacific is warmer, the southwest monsoon is stronger. This is different from the case on the interannual timescale, where the southwest monsoon is usually weaker than normal during El Niño events.

Acknowledgments

We are thankful to Prof. Shaowu Wang, Prof. Guoxiong Wu, Mr. Luke He, Prof. Zhenguo Zhao, and Dr. Jinlin Ye for providing data and discussions, and to Dr. Suhung Shen for her EOF code. We are grateful to Prof. Jun Matsumoto for his many thoughtful suggestions. This work was supported by the Global Modeling and Analysis Program and the Earth Observing System Interdisciplinary Investigation Program of the NASA/Office Mission to Planet Earth.

References

Bretherton, C.S., C. Smith and J.M. Wallace, 1992: An intercomparison of methods for finding coupled patterns in climate data. *J. Climate*, **5**, 541–560.

Chen, L.-X., Y.-N. Shao and Z.-H. Ren, 1994: Climate change in China during the past 70 years and its relationship to the variation of monsoon. R. G. Zepp (ed.), *Climate-Biosphere Interaction*, Wiley and Sons, 31–50.

Graham, N.E., 1994: Decadal-scale climate variability in the 1970's and 1980's: Observations and model results. *Clim. Dyn.* **10**, 135–162.

Gu, D. and S.G.H. Philander, 1997: Interdecadal climate fluctuations that depend on exchanges between the tropics and extratropics. *Science*, **275**, 805–807.

Hu, Z.-Z., 1997: Interdecadal variability of summer climate over East Asia and its association with 500 hPa height and global sea surface temperature. *J. Geophys. Res.*, **102**, 19403–19412.

Kawamura, R., 1994: A rotated EOF analysis of global sea surface temperature variability with interannual and interdecadal scales. *J. Phys. Oceanog.*, **24**, 707–715.

Kleeman, R., R.A. Colman, N.R. Smith and S.B. Power, 1996: A recent change in the mean state of the Pacific basin climate: observational evidence and atmospheric and oceanic responses. *J. Geophys. Res.*, **101**, 20483–20499.

Lau, K.-M. and M.-T. Li, 1984: The monsoon of East Asia and its global associations—A survey. *Bull. Amer. Meteor. Soc.*, **65**, 114–125.

Lau, K.-M. and H.-Y. Weng, 1995: Climate signal detection using wavelet transform: How to make a time series sing. *Bull. Amer. Meteor. Soc.*, **76**, 2391–2402.

Lau, K.-M. and H.-Y. Weng, 1999: Interannual, interdecadal and global warming signals in sea surface temperature. *J. Climate*, **12**, 1257–1267.

Li, C.-Y. and Q.-H. Liao, 1998: The quasi-decadal oscillation of air-sea system in the northwestern Pacific region. *Adv. Atmos. Sci.*, **15**, 31–40.

Liang, Y.-L., J.-C. Song and X.-C. Wang, 1992: Variations of drought and flood during summer monsoon active seasons in China and its impact. J.-J. Zhang

and R.-H. Huang (eds.), *Studies of long term weather forecast and the sun-earth relationship*, Ocean Press, 165–173 (in Chinese).

Minobe, S., 1997: A 50–70 year climatic oscillation over the North Pacific and North America. *Geophys. Res. Lett.*, **24**, 683–686.

Nitta, T., 1987: Convective activities in the tropical western Pacific and their impact on the Northern Hemisphere summer circulation. *J. Meteor. Soc. Japan*, **65**, 373–390.

Nitta, T. and Z.-Z. Hu, 1996: Summer climate variability in China and its association with 500 hPa height and tropical convection. *J. Meteor. Soc. Japan*, **74**, 425–445.

North, G.R., 1984: Empirical orthogonal functions and normal modes. *J. Atmos. Sci.*, **41**, 879–887.

Simmonds, I., D. Bi and B. Yan, 1996: Relationships between summer rainfall over China and ocean temperatures in the tropical western Pacific. *J. Meteor. Soc. Japan*, **74**, 273–279.

Trenberth, K.E., 1990: Recent observed interdecadal climate changes in the Northern Hemisphere. *Bull. Amer. Meteor. Soc.*, **71**, 988–993.

Trenberth, K.E., 1997: The definition on El Niño. *Bull. Amer. Meteor. Soc.*, **78**, 2771–2777.

Trenberth, K.E. and J.W. Hurrel, 1994: Decadal atmosphere-ocean variations in the Pacific. *Clim. Dyn.*, **9**, 303–319.

Wallace, J.M., C. Smith and C.S. Bretherton, 1992: Singular value decomposition of wintertime sea surface temperature and 500-mb height anomalies. *J. Climate*, **5**, 561–576.

Webster, P.J. and S. Yang, 1992: Monsoon and ENSO: selectively interactive system. *Quart. J. Roy. Meteor. Soc.*, **118**, 877–926.

Weng, H.-Y. and K.-M. Lau, 1994: Wavelets, period doubling, and time-frequency localization with application to organization of convection over the tropical western Pacific. *J. Atmos. Sci.*, **51**, 2523–2542.

Wu, G.-X. and H.-Z. Liu, 1995: Neighborhood response of rainfall to tropical sea surface temperature anomalies. Part I. Numerical experiment. *Chinese J. Atmos. Sci.*, **19**, 279–292.

Wu, G.-X., F.-Y. Sun, J.F. Wang, and X.-C. Wang, 1995: Neighborhood response of rainfall to tropical sea surface temperature anomalies. Part II. Data analysis. *Chinese J. Atmos. Sci.*, **19**, 375–389.

Yatagai, A. and T. Yasunari, 1995: Interannual variations of summer precipitation in the arid/semi-arid regions in China and Mongolia: their regionality and relation to the Asian summer monsoon. *J. Meteor. Soc. Japan*, **73**, 909–923.

Zhang, Y., J.M. Wallace and D.S. Battisti, 1997: ENSO-like interdecadal variability: 1900–93. *J. Climate*, **10**, 1004–1020.

中国における夏の降水量の様々な時間スケールでの変動およびその長期変動と全球海面水温変動との関係

翁　衡毅・劉　家銘
(Laboratory of Atmosphere, NASA/GSFC)
薛　永康
(Department of Geography, University of Maryland)

中国における夏（6–8月）の降水量の様々な時間スケールでの変動、およびその長期変動とグローバルな海面水温（SST）変動との関係を、1955–97年の期間について調べた。まず、降水量変動に卓越する時空間パターンを、EOF解析により明らかにした。EOFの第1・第2成分をウェーブレット解析した結果、年々変動・10年～数十年周期変動・長期トレンドの各周期の変動が認められた。EOFの第1成分では、1970年代後半に中国における急激な降水量分布の変化が認められ、1980年代には華中東部で湿潤、華北と華南で乾燥となる傾向が、1960年代に比べて強くなった。この急激な変化は、20年および40年程度の長い時間スケールでの変動が、ほぼ同時に位相変化したことに伴って生じている。EOFの第2成分では、華中および華南の広い範囲で、降水量の増加トレンドが認められ、とくに揚子江流域でこの傾向は顕著である。この成分には、1970年代の後半の急激な変化は認められない。これは長期的なトレンドと20年スケールでの変動の位相があわず、それらの変動が相殺しあったため、と考えられる。

次に、グローバルな海面水温（SST）変動と関係する中国の降水量の長期変動を理解するために、この2つを場を特異値分解解析（SVD）によって解析した。SVDの第1成分では、華北の乾燥・華中の大雨傾向は、エルニーニョ的なSST偏差分布と関係していることがわかった。この成分には、降水量のEOF成分では同時に現われることがなかった、長期トレンドおよび1970年代後半における急激な変化が、ともに認められた。SVDの第2成分では、揚子江と黄河の間の地域での降水量の不足（過多）と、東部太平洋での波動状のSST偏差分布、すなわち、熱帯と中緯度地域における負（正）偏差と、北アメリカ西岸沖の亜熱帯域での正（負）偏差が関係していることが示された。SVDの第3成分によると、揚子江河谷での降水量変動は、北緯20度・東経140度を中心とする西太平洋におけるSSTと関係している。中国各地の降水量分布は、SSTの影響によって現われるとみられるこれらのSVD成分の、相殺や強化の結果として現われるものと考えられる。SVD解析によって見い出されたもっとも重要な関係は、クロス相関解析によっても確認された。最後に長期トレンドスケールで、大規模循環場の変化に伴い、中国の降水量とグローバルなSSTが変化するシナリオを提示した。